Computational and Structural Biotechnology Journal 20 (2022) 2070–2081

COMPUTATIONAL AND STRUCTURAL BIOTECHNOLOGY JOURNAL

journal homepage: www.elsevier.com/locate/csbj

Structural characterization of a cross-protective natural chimera of factor H binding protein from meningococcal serogroup B strain NL096

Daniele Veggi [1,*], Enrico Malito [1,2], Paola Lo Surdo, Werner Pansegrau, Valentina Rippa, Newton Wahome, Silvana Savino, Vega Masignani, Mariagrazia Pizza, Matthew J. Bottomley

GSK Vaccines srl, Via Fiorentina 1, Siena 53100, Italy

ARTICLE INFO

Article history:
Received 30 March 2021
Received in revised form 11 April 2022
Accepted 11 April 2022
Available online 18 April 2022

ABSTRACT

Invasive meningococcal disease can cause fatal sepsis and meningitis and is a global health threat. Factor H binding protein (fHbp) is a protective antigen included in the two currently available vaccines against serogroup B meningococcus (MenB). FHbp is a remarkably variable surface-exposed meningococcal virulence factor with over 1300 different amino acid sequences identified so far. Based on this variability, fHbp has been classified into three variants, two subfamilies or nine modular groups, with low degrees of cross-protective activity. Here, we report the crystal structure of a natural fHbp cross-variant chimera, named variant1-2,3.x expressed by the MenB clinical isolate NL096, at 1.2 Å resolution, the highest resolution of any fHbp structure reported to date. We combined biochemical, site-directed mutagenesis and computational biophysics studies to deeply characterize this rare chimera. We determined the structure to be composed of two adjacent domains deriving from the three variants and determined the molecular basis of its stability, ability to bind Factor H and to adopt the canonical three-dimensional fHbp structure. These studies guided the design of loss-of-function mutations with potential for even greater immunogenicity. Moreover, this study represents a further step in the understanding of the fHbp biological and immunological evolution in nature. The chimeric variant1-2,3.x fHbp protein emerges as an intriguing cross-protective immunogen and suggests that identification of such naturally occurring hybrid proteins may result in stable and cross-protective immunogens when seeking to design and develop vaccines against highly variable pathogens.

1. Introduction

Neisseria meningitidis is a leading cause of meningitis and sepsis worldwide [1–2]. Despite available antibiotic therapies, *N. meningitidis* causes considerable morbidity and mortality; across Europe in 2017, there were 3221 cases reported of invasive meningococcal disease and 282 associated deaths [3]. Highly-effective glycoconjugate vaccines have been available for many years to protect against meningococcal serogroups A, C, W135, and Y [4]. In contrast, many years of research and new technologies were needed, including the development of the 'Reverse Vaccinology' approach [5], to have two different recombinant protein vaccines against meningococcus serogroup B (MenB) available, both of which contain the factor H binding protein (fHbp) as a key immunogen [6–8].

fHbp is a 28 kDa surface-exposed meningococcal lipoprotein, with a three-dimensional (3D) structure exhibiting two β-barrel domains connected by a short linker [9–11]. During infection, fHbp binds the human complement regulatory factor H (hfH) on the bacterial surface, and inhibits activation of the complement alternative pathway [12]. Hence, fHbp mediates one of several immune evasion mechanisms, which allow the bacteria to multiply in blood and cause sepsis [12]. fHbp molecules are included in both licensed recombinant protein MenB vaccines (4CMenB (Bexsero) and MenB-fHbp (Trumenba)) and elicit antibodies with complement-mediated bactericidal activity [6]. Over 1300 different amino acid sequence variants of fHbp have been reported to date [13], and can be sorted by sequence into three distinct 'variant groups' [14], or two subfamilies [15], or nine modular groups [16–17]. Accordingly, any single fHbp variant induces antibodies with bactericidal activity [18–19] against strains expressing similar subvariants (usually sharing at least 80% identity in fHbp sequence), but with very low or no 'cross-protective' activity against strains expressing different fHbp subvariants with lower sequence identity.

* Corresponding author at: GSK Vaccines srl, Via Fiorentina 1, Siena 53100, Italy.
E-mail address: daniele.x.veggi@gsk.com (D. Veggi).
[1] These authors contributed equally to this work.
[2] Current address: Schrödinger, Inc., New York City, New York 10036, USA.

https://doi.org/10.1016/j.csbj.2022.04.011

From the vaccine viewpoint, the challenges of fHbp antigen sequence variability can be overcome by the inclusion of additional antigens in multicomponent vaccines, as in the case of 4CMenB, which includes the *Neisseria* Heparin binding Antigen (NHBA) and *Neisseria* Adhesin A (NadA) in combination with outer membrane vesicles from the New Zealand outbreak strain (NZ 98/254). Also, the identification of key epitopes recognized by bactericidal anti-fHbp antibodies has allowed the rational design of chimeric fHbp antigens which contain epitopes expressed by all three variant groups, and these engineered antigens induced antibodies in mice with cross-bactericidal activity [20–22]. These studies show that structure-based design of bacterial antigens can result in the generation of broadly protective vaccines. Moreover, similar 'Structural Vaccinology' approaches have proven successful in the rational design of viral antigens with enhanced stability and immunogenicity in preclinical and clinical testing [23–27], particularly relevant for difficult targets that previously eluded standard vaccine development methods.

Phylogenetic analyses based on multiple entire amino acid sequences suggested that the *fHbp* gene has evolved through horizontal transfer and recombination, and this drove sequence classification on the basis of modular groups [28]. Extensive fHbp sequence analysis based on this modular composition identified a natural chimera, classified as group IV, which accounted for 23 % of UK isolates, <1 % of U.S. isolates and 6 % of isolates in France. It was speculated that the high proportion of isolates carrying a group IV natural chimera in UK might reflect the recent emergence of group B strains from the ST-269 clonal complex [17]. Moreover, two unusual chimeras were isolated in the Netherlands, one of which derived from a MenB strain (NL096) isolated in 1960 [29]. On the basis of sequence, the fHbp antigen produced by the NL096 strain was defined as fHbp variant1-2,3.x, because its N-terminal domain sequence most closely resembled variant1 (97 % amino acid sequence identity, compared to only 77 % or 61 % sequence identity when compared with variant2 or variant3), while its C-terminal domain sequence resembled variants2/3 (87/80 % identity, compared to only 71 % identity with variant1).

Remarkably, when twelve sequence-diverse recombinant fHbp antigens representing variants 1, 2 or 3 were tested in mice, only fHbp variant1-2,3.x raised a serum antibody response that exhibited strong bactericidal activity against representative MenB strains displaying fHbp molecules from across all three variant groups [30]. Here we describe the biochemical, biophysical, and structural features of the fHbp variant1-2,3.x chimera. This is the first study showing the peculiarities of a chimeric fHbp antigen "designed by Nature". Our in-depth characterization of the interplay between sequence, structure and function shed light on the functional and immunological properties of this natural chimera and may guide the design of even more powerful immunogens.

2. Results

2.1. fHbp variant1-2,3.x shows favorable thermostability

Thermostability is an important characteristic of recombinant proteins intended for use in medicines or vaccines and, moreover, thermostability has been positively correlated with immunogenicity of vaccine antigens [31–32]. It is known that the N-terminal domain of fHbp variant1 is considerably more thermostable than that of variant2 or variant3 [33–34]. Indeed, a rationally-designed fHbp variant2 mutant engineered with higher N-terminal domain thermostability [35] was shown to have improved immunogenicity in mice [36]. To examine the thermostability of the chimeric fHbp variant1-2,3.x protein, we compared its behaviour with the wild-type variant1, variant2 and variant3 proteins using differential scanning calorimetry (DSC). The purified recombinant 1–2,3.x protein displayed a DSC thermogram with two peaks, indicating melting temperature midpoints (T_m) of 68 ± 0.5 °C (341 K) and 90 ± 0.5 °C (363 K) which, by analogy with all other fHbp proteins studied, correspond to the N- and C-terminal domain unfolding events, respectively (Fig. 1) [34]. The variant1-2,3.x protein was therefore found to be comprised of two highly stable folded domains; it is at least as stable as fHbp variant1 and, importantly, its N-terminal domain is considerably more stable than that found in fHbp variant2 and somewhat more stable than that in variant3. This biophysical data demonstrates that the variant1-2,3.x protein naturally combines the favourable thermostability features of the fHbp variant1 N-terminal domain and the fHbp variant2/3 C-terminal domain.

2.2. First atomic resolution structure of fHbp

The DSC data for fHbp 1–2,3.x revealed promising thermostability features of the distinct N- and C-terminal domains; however, the three-dimensional (3D) structure of this chimeric fHbp was unknown. In particular, given the apparent genetic merging of fHbp N- and C-terminal domains arising from distinct and divergent MenB strains, we sought to determine whether both the individual domains and moreover the N-terminal/C-terminal domain interface in variant1-2,3.x could assume the typical conformations and relative intramolecular orientations of other known fHbp structures and, if so, how this might impact hfH-binding function. To this end, first, we determined the X-ray crystallographic structure of variant1-2,3.x, using the molecular replacement (MR) method. The crystal structure was refined to 1.2 Angstrom (Å) resolution (Table 1) and is therefore by far at the highest resolution of the nineteen fHbp 3D structures reported to date (Table 2) [37]. Extremely high-quality electron density maps were obtained (Fig. 2), enabling confident model building. Indeed, at such high resolution, in addition to building the entire polypeptide chain of v1-2,3.x in the sequence range G15-Q255 (with the exception of the short β7-β8 loop residues 118–122, for which only poor density was observed likely due to local disorder; note, the residue numbering system used is based on the mature protein sequence beginning with the lipidated cysteine of fHbp variant1.1), it was also possible to observe hundreds of bound water molecules and several sulfate buffer molecules (Fig. 2, boxes).

The 3D structure of variant1-2,3.x was revealed to be composed of an N-terminal taco-shaped β-sheet domain (essentially an incomplete β-barrel) and a C-terminal β-barrel domain (complete), and therefore presents the typical domain structure of known fHbp proteins (Fig. 3AB). The structural superposition of fHbp variant1-2,3.x with each of the three known fHbp variants revealed very high similarity, as indicated by low root mean square deviation (r.m.s.d.) values for all 240 aligned alpha carbon backbone atoms (r.m.s.d. values of 0.67, 0.63 and 0.72 Å when compared with fHbp variant1, 2 and 3, respectively). Moreover, the N- and C-terminal domains show the canonical relative domain orientation, presenting the same cross-interface domain-domain interactions as observed for known fHbp variant1, variant2 and variant3 proteins. Interestingly, although the C-terminal domain of variant1-2,3.x shows numerous sequence differences from variant1, an analysis of the crystal structure revealed that most of the residues (approx. 50) that make contacts across the domain-domain interface are conserved in fHbp variant1, variant2, variant3 and variant1-2,3.x (Fig. 3C-E), suggesting that conservation of both the structure and the relative orientation of the N- and C-terminal domains are essential for biological function.

Upon its initial discovery, sequence analyses indicated that fHbp variant1-2,3.x was a hybrid protein likely generated by horizontal gene transfer events common in pathogenic *Neisseria* [30],

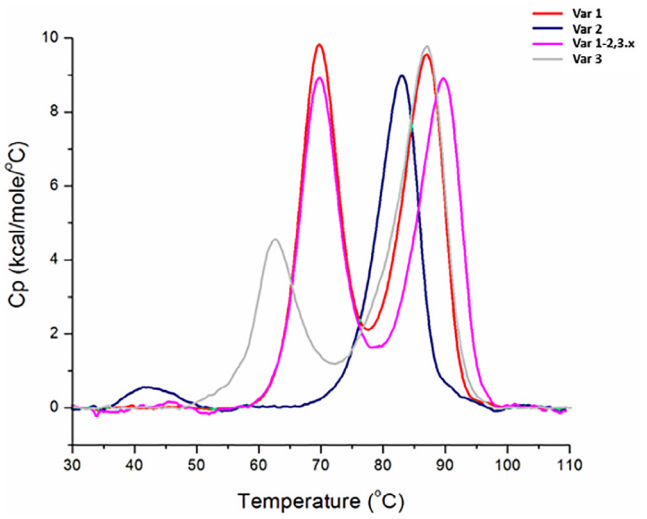

Fig. 1. DSC thermogram of fHbp variant1-2,3.x (magenta) reveals two major peaks (T_m values 68 °C (341 K) and 90 °C (363 K)) similar to variant1 (red). The N-terminal domain unfolding transitions for variant2 (blue) and variant3 (grey) occur at lower temperatures (approx. 42 °C (315 K) and 62 °C (335 K), respectively).

Table 1
Data collection and refinement statistics for the fHbp variant1-2,3.x crystal structure.

Wavelength	0.99987
Resolution range (Å)	23.19–1.22 (1.264–1.22)
Space group	C 1 2 1
Unit cell	125.68 42.61 44.41 90 100.2 90
Total reflections	197,875 (27900)
Unique reflections	68,964 (9280)
Multiplicity	3.0 (3.0)
Completeness (%)	95.2 (92.4)
Mean I/sigma(I)	10.5 (4.4)
Wilson B-factor	10.19
Matthews coefficient (solvent content)	2.15 (42.88 %)
No. of molecules in the ASU	1
R-merge	0.06 (0.20)
R-meas	0.08 (0.24)
Reflections used in refinement	65,644 (2495)
Reflections used for R-free	3315 (120)
R-work	0.1418 (0.1592)
R-free	0.1659 (0.1756)
Number of non-hydrogen atoms	2170
protein	1896
ligands	11
water	322
Protein residues	239
RMS (bonds)	0.011
RMS (angles)	1.16
Ramachandran favoured (%)	97
Ramachandran allowed (%)	3.2
Ramachandran outliers (%)	0
Rotamer outliers (%)	0
Clashscore	3.4
Average B-factor	15.77
macromolecule	14.24
ligands	15.85
solvent	26.72

Statistics for the highest-resolution shell are shown in parentheses.
ASU: asymmetric unit.

as also noted previously in studies of the modular architecture of fHbp proteins and inter-subfamily recombination [16,38]. Indeed, when comparing the N- and C-terminal domain structures separately, the fHbp variant1-2,3.x N-terminal domain was structurally most similar to variant1, whereas the variant1-2,3.x C-terminal domain was structurally most similar to variant2 (Fig. 3A-C). The

Table 2
List of fHbp-containing crystal structures deposited in the PDB, ordered by resolution, current at 29 Mar 2021.

fHbp var.	Resolution (Å)	PDB code	Co-crystallized*
1–2,3.x	1.22	7NRU	–
2.22	1.62	4Z3T	–
1.1	1.63	5NQZ	–
1.1	1.80	2YPV	mFab 12C1
1.1	1.90	2Y7S	–
1.1	2.00	3KVD	–
1.1	2.19	5O14	huFab 1A12
3.28	2.31	4AYI	hfH CCPs 6–7
1.1	2.35	2 W80	hfH CCPs 6–7
1.1	2.35	2 W81	hfH CCPs 6–7
1.1	2.39	6XZW	huFab 4B3
1.1	2.40	4AYD	hfH CCPs 6–7
1.4	2.6	5NQY	–
3.28	2.65	6H2Y	huFab 1E6
1.1	2.80	4AYE	hfH CCPs 6–7
3.28	2.85	4AYM	hfH CCPs 6–7
1.4	2.86	5NQP	–
1.1	2.98	5T5F	mFab JAR5
1.1	3.66	5NQX	–

* The abbreviation mFab indicates murine (m) Fragment antibody binding (Fab), while huFab indicates a human Fab was used for co-crystallization. The PDB code provides links to the atomic coordinates and structure factors held at the Protein Data Bank (https://www.wwpdb.org), and in turn to any accompanying publications.

structural data presented here experimentally confirm the sequence-based predictions, and concretely demonstrate that fHbp variant1-2,3.x has the conserved structural features of all known fHbp proteins, notwithstanding its unusual hybrid genetic origin.

2.3. fHbp variant1-2,3.x presents combined antigenic surface features from fHbp variants

In addition to understanding the global 3D backbone, domain interface, and side chain structural relationships between variant1-2,3.x and the fHbp variants 1, 2 and 3, we sought to explore their antigenic relationships; i.e. how similar are these proteins when considering solely their surface-exposed residues available as immunogenic epitopes? Would one expect the N-terminal domain of variant1-2,3.x to elicit the same immune response as the N-terminal domain of fHbp variant1, and likewise would the C-terminal domain of variant1-2,3.x elicit the same immune response as the C-terminal domain of fHbp variant2 or variant3? Therefore, we analysed pairwise structural alignments to compare specifically the immunogenic surfaces, firstly comparing the N-terminal domain of variant1-2,3.x with variant1, and secondly comparing the C-terminal domain of variant1-2,3.x with variant2 and variant3 (Fig. 4). In the N-terminal domains compared, only four residues differed, corresponding to mutations Q87K, F109L, I114V and H119D (nomenclature format here is variant1/residue number/variant1-2,3.x). When mapped to the structure, residue L109 appears fully buried, while residue V114 is partially buried, and residues K87 and D119 are fully solvent exposed. The latter three mutations therefore likely generate slightly different antigenic properties on variant1-2,3.x compared to variant1, but which are localized in a small surface area when compared to the overall total protein surface, suggesting that the variant1-2,3.x N-terminal domain could elicit an immune response very similar (almost identical) to that elicited by the N-terminal domain in fHbp variant1 (Fig. 4A). Intriguingly, in patients with meningococcal meningitis, the presence of the N-terminal domain Aspartate (Asp, D) at position 119 (termed residue D184 in the alternative numbering system) was found to be associated with increased risk of septic

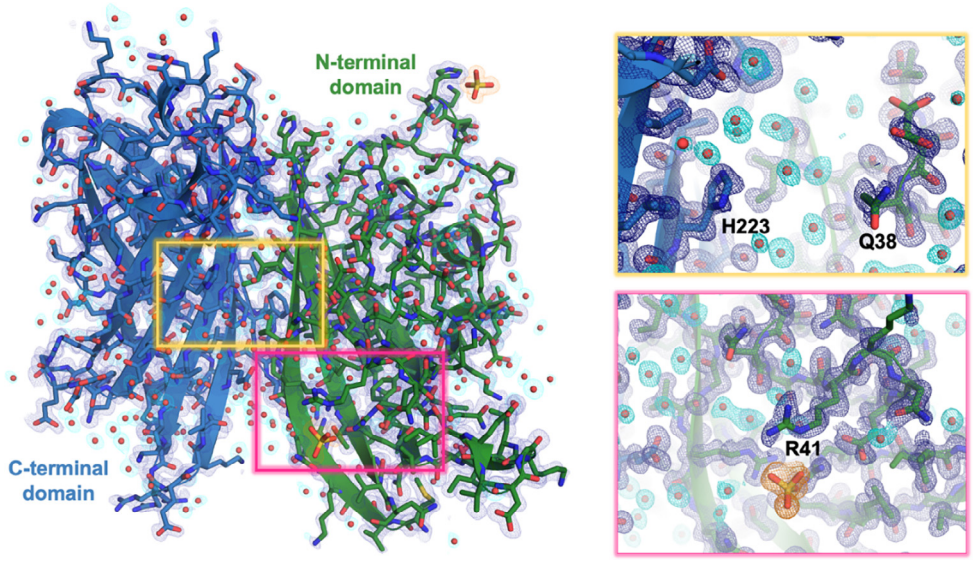

Fig. 2. High-quality electron density maps obtained from the crystallographic data of fHbp variant1-2,3.x refined to 1.2 Å resolution. The structure revealed the overall 3D fold (left) and allowed visualization of protein side chains, water and buffer molecules (sulfates) from the crystallization media, as shown in the boxes. Blue, cyan, and orange meshes show sigma-A-weighted 2Fo-Fc electron density maps for the fHbp protein, water, and sulfates, respectively, with a contour level of 1σ. The backbone cartoon ribbon and side chain sticks are colored green for the N-terminal domain, blue for the C-terminal domain; red spheres show water. Boxes of enlarged areas show labelled residues of interest which were mutated later in this study, as discussed below.

shock during admission, resulting in more frequent unfavourable outcomes [29]. This observation suggests that the region around residue 119 is an important antigenic functional site. As such, the NL096 strain might have an evolutionary advantage, and an immunogen carrying D119 might provide greater protection against such virulent strains.

We performed a similar molecular analysis of the fHbp C-terminal domains, and found that variant1-2,3.x has 14 total residues that differ when compared to fHbp variant2. When mapped to the surface of variant1-2,3.x, all these residues appear at least partially solvent-exposed (Fig. 4B). Furthermore, variant1-2,3.x has 24 residues that differ when compared to fHbp variant3, many of which map to solvent exposed sites (Fig. 4C). However, given that the total solvent-exposed surface on the C-terminal domains of fHbp variants is large (~7,000 Å [2], calculated using PISA [39]) and comprised of many of > 110 residues in the C-terminal domain, the variant1-2,3.x would be expected to exhibit a similar immunogenic profile to variant2 and variant3, with some differences due to mutations in localized patches.

We also examined the variant1-2,3.x sequence to verify the presence of epitope residues seen in previous co-crystal structures of fHbp with three quite different cross-reactive human mAbs 1A12 [40], 1E6 [41] and 4B3 [42]. The 1A12 epitope is located exclusively on the C-terminal domain, at one end (a small face) of the β-barrel [40]. In contrast, the 1E6 epitope spans both the N- and C-terminal domains and lies on the face opposite to the hfH binding site [41]. The 4B3 epitope is found exclusively on the C-terminal domain, occupying one side (a long face) of the β-barrel and partially overlapping with the hfH binding site [42]. These epitopes are comprised of 16 or 17 residues, mostly discontinuous, which share 56, 63 and 71 % sequence identity (and greater similarity) respectively with variant 1–2,3.x. The high degree of spatially co-localized sequence conservation suggests that the chimera might also bind to these human mAbs, though not necessarily with the same high affinity (sub-nanomolar values of the equilibrium dissociation constant, K_D), and by corollary might also be capable of eliciting such mAbs in humans.

2.4. Molecular basis of lower hfH binding affinity in fHbp 1–2,3.x compared to variant1

In addition to influencing immunogenicity, the surface properties of fHbp also influence its ability to bind human factor H (hfH), which in turn allows bacterial growth in blood, leading to sepsis [12]. To date, all meningococcal fHbp variants tested have shown an ability to bind hfH with relatively high affinity, exhibiting equilibrium dissociation constants (K_D) typically in the low nanomolar range. Seib *et al.* tested twelve different fHbp variants in a surface plasmon resonance (SPR) assay and found K_D values that ranged from 7 to 350 nM [30]. Notably, in that study, variant1-2,3.x was reported to bind hfH approximately 4-fold weaker than variant1. However, since the K_D values in that early study for which replicate and standard deviations were reported exhibited relatively high variability (see Table 3, therein), we repeated the binding experiment using a more advanced instrument potentially more sensitive and precise (i.e. Biacore T200 rather than Biacore X100). We found that variant1-2,3.x bound to hfH with K_D = 30.4 ± 1.0 nM, approximately 1.34-fold weaker than variant1 (K_D = 22.7 ± 0.5 nM) (Fig. 5).

While the difference in K_D values is smaller than reported previously [30], our SPR experiments confirmed that variant1-2,3.x binds to hfH more weakly than variant1.1. The NL096 strain expresses high amounts of fHbp [30], and it is plausible that this quantity compensates functionally for its lower affinity, thereby recruiting sufficient hfH to enable immune evasion. Here, we sought to elucidate the molecular basis of the different affinities of variant1-2,3.x and variant1 by comparing the interfacing residues between the fHbp variants and hfH, using the experimentally determined structures, a homology model of the variant1-2,3.x-hfH complex, manual inspection and computational analyses.

Using PISA [39] software on the fHbp variant1-hfH complex (PDB 2w80), thirteen residues of fHbp variant1 were found to make H-bonds or salt bridges with hfH. Of these, only 4 residues differ between variant1 and variant1-2,3.x: fHbp residues 209, 221 and 239 in the C-terminal domain, and residue 119 in the N-terminal domain. While the conservative S221T mutation (nota-

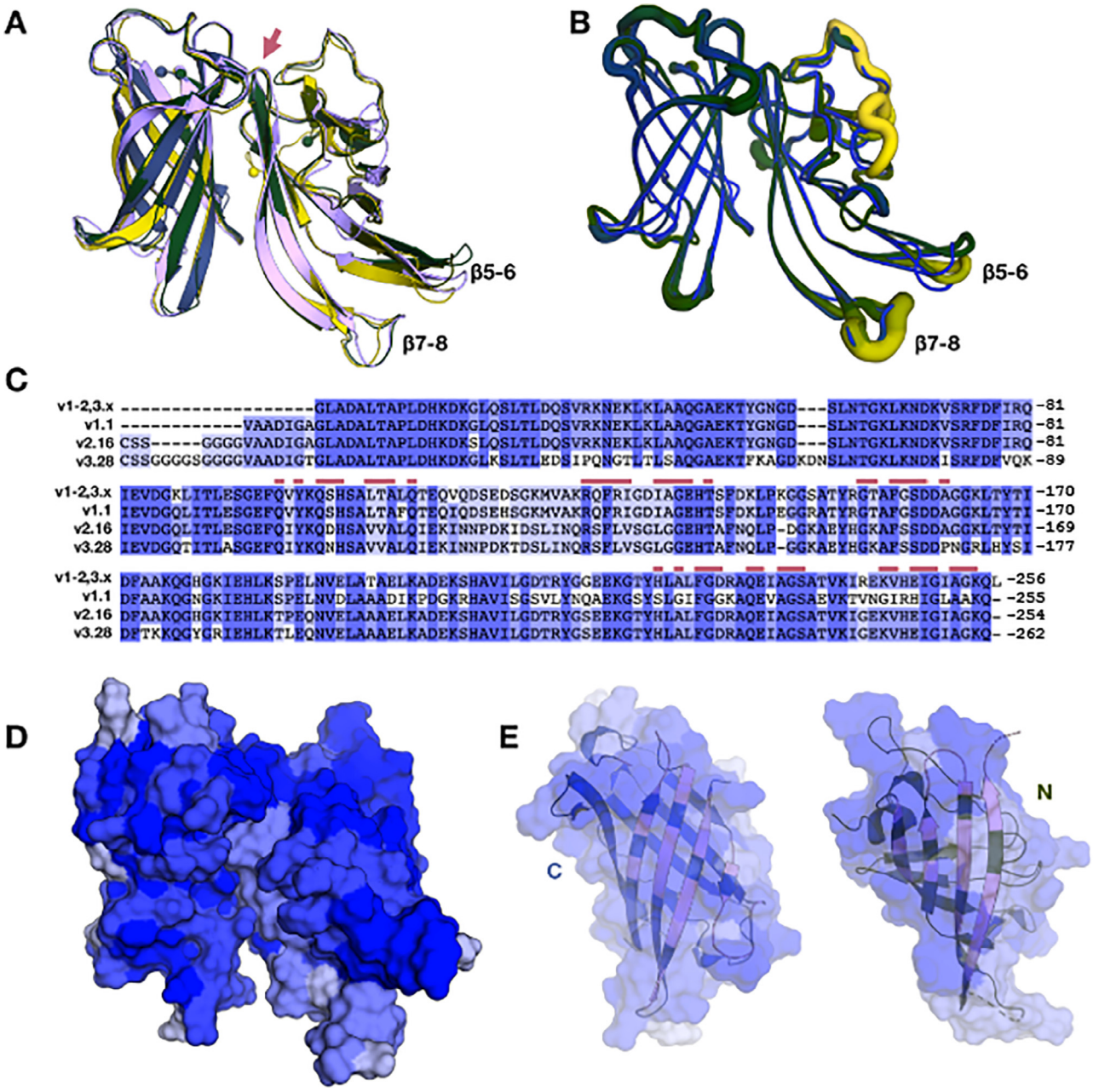

Fig. 3. The topology and relative domain orientations of fHbp variant1-2,3.x are highly conserved. **A**) Cartoons of variant1-2,3.x showing N-terminal domain (G15-G136, green) and C-terminal domain (T139-Q255, blue), superimposed onto fHbp variant1 (cyan, PDB 3kvd), variant2 (yellow, PDB 4z3t) and variant3 (magenta, PDB 4ayi). A red arrow marks the inter-domain linker (residues 137–138). The fHbp variant1-2,3.x N-terminal domain is structurally most similar to variant1 (r.m.s.d. 0.41 Å, compared to 0.54 Å and 0.68 Å for variant2 and variant3), whereas the variant1-2,3.x C-terminal domain is structurally most similar to variant2 (r.m.s.d. 0.29 Å, compared to 0.39 Å and 0.41 Å for variant3 and variant1, respectively). The most notable structural deviations are likely due to flexibility in the protruding N-terminal domain loops β5-6 (labelled), and disorder (resulting in lack of electron density) in loops β7-8 of variant1-2,3.x. **B**) Cartoon putty representations of the superpositions in panel A), colored by B-factors and with greater diameter indicating higher B-factors (flexibility/disorder). **C**) Sequence alignment of all four fHbp variants shown in A, with red bars indicating residues involved in the N-/C-terminal domains interface. **D**) Surface representation of fHbp variant1-2,3.x colored according to sequence conservation with fHbp variants 1, 2, and 3 (a blue gradient, where white = non-conserved, dark blue = conserved). **E**) Open-book views of fHbp v1-2,3.x to reveal conservation at the N-/C-terminal interface, with contacting residues colored in red on the cartoon ribbon, corresponding to the red bars of panel C.

tion is such that S is in variant1.1 and T is in variant1-2,3.x, etc.) is not expected to greatly alter the overall bonding network, two less conservative mutations likely lead to loss of bonds with hfH: the fHbp mutation S209L removes an H-bond with the hfH Met340 carbonyl group and, most notably, the fHbp mutation E239T removes a salt bridge to the hfH Arg341 side chain (Fig. 6 BC). Similarly, the sole fHbp N-terminal domain mutation, H119D, introduces a side chain charge inversion that likely removes or weakens interactions with hfH His402 and Gly403 main chain atoms (Fig. 6 DE).

Additionally, manual inspections revealed how fHbp variant1 residues Ser223 and His248 are also involved in binding to hfH. Here, the variant1-2,3.x mutations S223H and H248E may contribute to reduced binding affinity, since fHbp H223 would not support an apparently extensive H-bonding network, and the negative potential introduced by fHbp E248 could potentially dis-

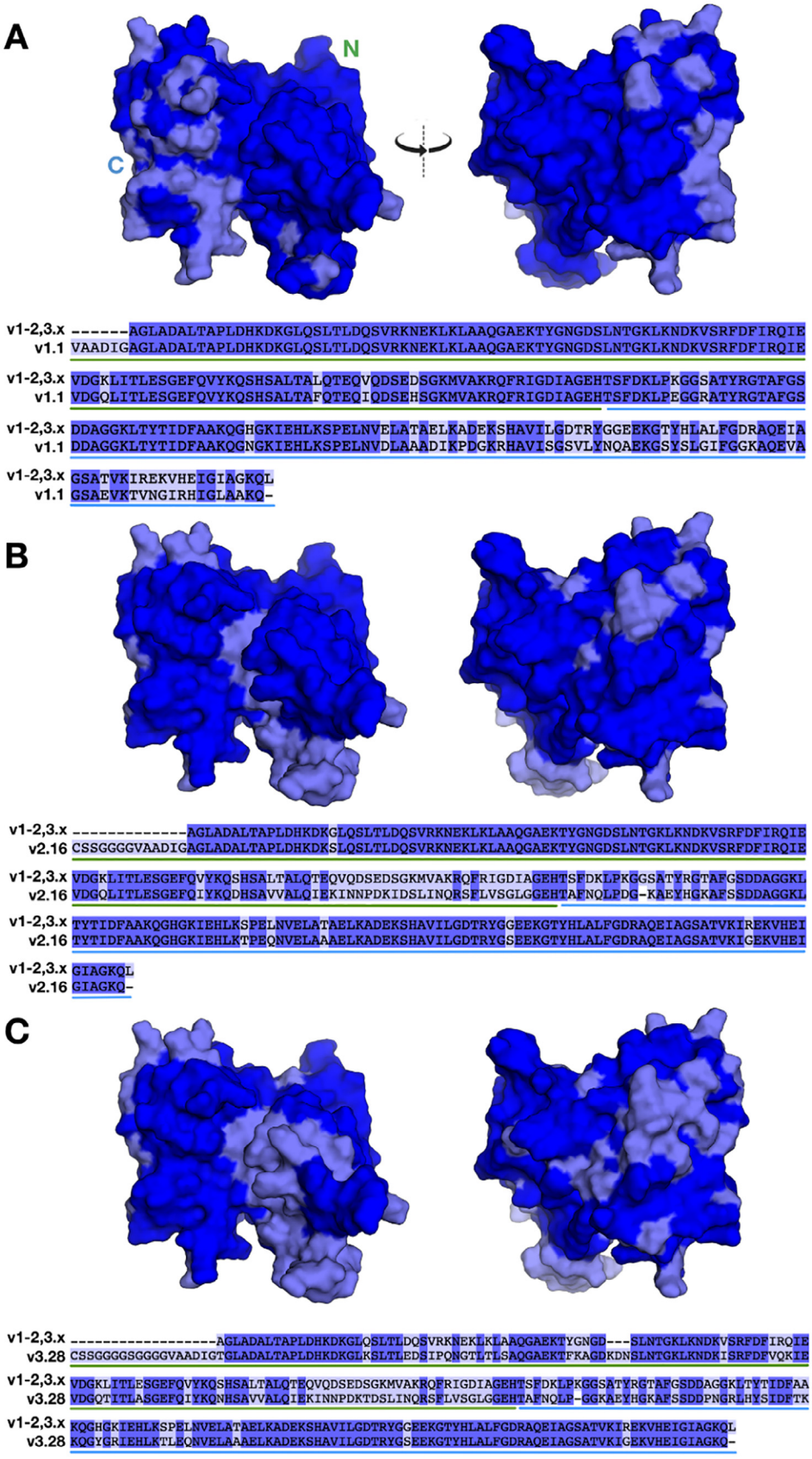

Fig. 4. Conservation of fHbp variant1-2,3.x immunogenic surface, as compared to fHbp variant1, 2, and 3. Surface plots of fHbp variant1-2,3.x colored according to pairwise sequence conservations (white to blue gradient) mapped on the structure after sequence/structure alignment with fHbp v1.1 (**A**), v2.16 (**B**), and v3.28 (**C**). Green and blue bars below the sequences indicate the N (green) and C (blue) terminal domains.

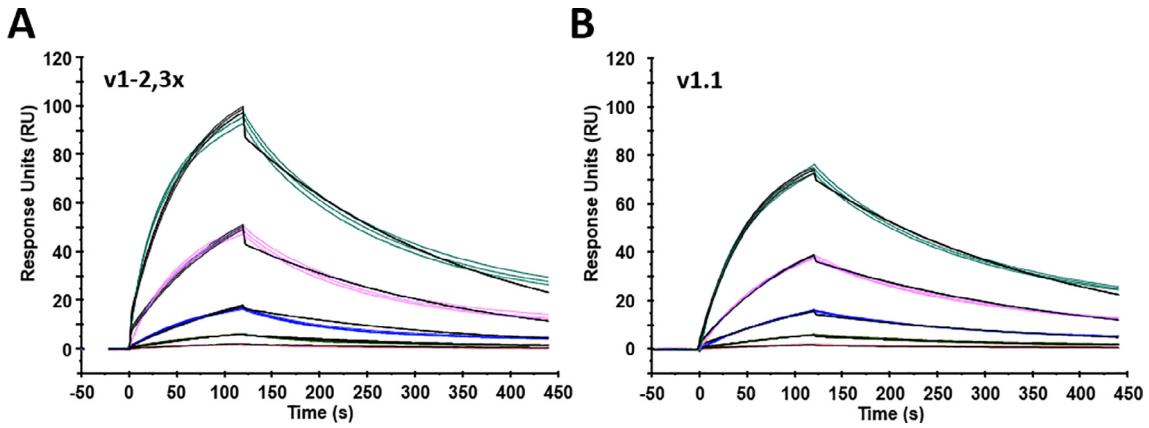

Fig. 5. SPR multi-cycle kinetic analysis of fHbp variants binding to immobilized hfH. **A, B)** Sensorgrams were acquired in triplicate with fHbp at 100 nM (turquoise), 33.3 nM (magenta), 11.1 nM (blue), 3.70 nM (green) and 1.23 nM (red) analyte concentration. Curves were fitted using the 1:1 binding model of interaction and resulting graphs are shown in black. **A)** Sensorgrams were obtained with fHbp v1-2,3x as analyte. **B)** Sensorgrams were obtained with fHbp v1.1 as analyte.

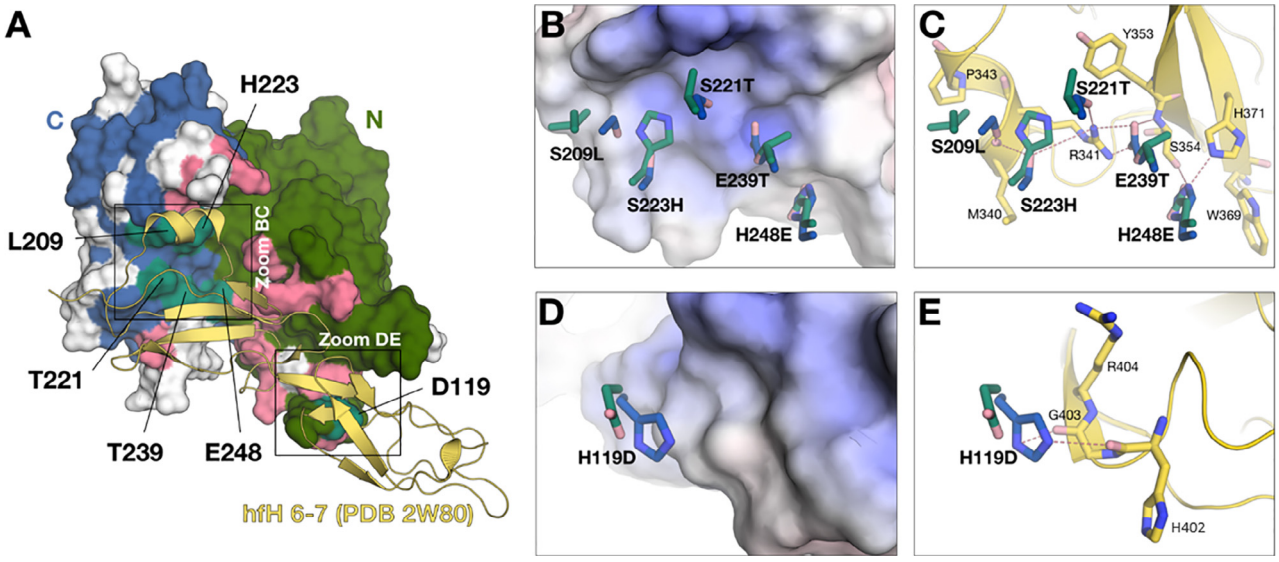

Fig. 6. Molecular basis for lower affinity of variant1-2,3.x for hfH. **A)** Homology model surface plot of variant1-2,3.x-hfH complex; N-terminal domain green, C-terminal domain blue; red/cyan patches show conserved/non-conserved interfacing residues (only those non-conserved are labeled). B,C) Magnified view of the region comprising the C-terminal domain mutations, with sticks depicting fHbp and surface depicting hfH. Dashes in C show identified interactions. Blue sticks: variant1; cyan sticks: variant1-2,3.x; yellow: hfH. **D,E)** Same view as in panels BC for the region of the N-terminal domain mutation H119D. The hfH surface plots in **B** and **D** are colored by electrostatic potential. Bold/larger fonts (panels A-E) label fHbp residues, smaller and non-bold fonts (panels C and E) label hfH residues.

favour interactions with hfH Ser354 and/or remove hydrophobic stacking with the nearby W369 (Fig. 6C).

To extend these analyses beyond punctate inspections of individual interfacing residues identified within the essentially static structure as revealed (albeit at high resolution) by x-ray crystallography, we performed detailed *in silico* biophysical studies of the two complexes using Rosetta comparative modelling (RosettaCM) [43] software. Thousands of molecular poses were iteratively calculated, and the top 100 models of both variant1 and variant1-2,3.x (ranked by folding stability and binding energy, *in silico*) were selected for interface analyses (Fig. 7A). Firstly, our analyses confirmed that variant1 possesses better energetics for hfH binding and complex folding stability. Overall, the top 100 models (ranked by folding stability) showed 2 kcal/mol lower binding energy (i.e. increased affinity) in variant1 relative to variant1-2,3.x (Fig. 7B), consistent with the reported higher affinity of variant1. Secondly, in agreement with the observations above, these computational analyses also revealed that the sequence differences in variant1-2,3.x-hfH complex generate on average a more hydrophobic than polar surface at the interface of all molecular poses, compared to variant1 (Fig. 7C-E), which may contribute to its reduced affinity for hfH. Nevertheless, in aqueous solution, proteins generally tend to bury hydrophobic regions and associate via van der Waals' interactions. At this specific interface, the presence of Leu209 in v1-2,3.x (rather than Ser209 in variant1) eliminates an H-bond to hfH but might allow beneficial van der Waals' interactions with proximal hydrophobic residues on hfH, such as Met340 and/or Tyr344. Determination of the v1-2,3.x/hfH co-crystal structure could be of future interest in order to verify these potential interactions empirically.

In summary, using both manual and computational analyses, five specific mutations in variant1-2,3.x were found to possibly underlie its observed reduced binding affinity for hfH compared with variant1, by the loss of distinct intermolecular interactions, several of which conferred an increased degree of hydrophobicity to the hfH binding interface present on variant1-2,3x. As such,

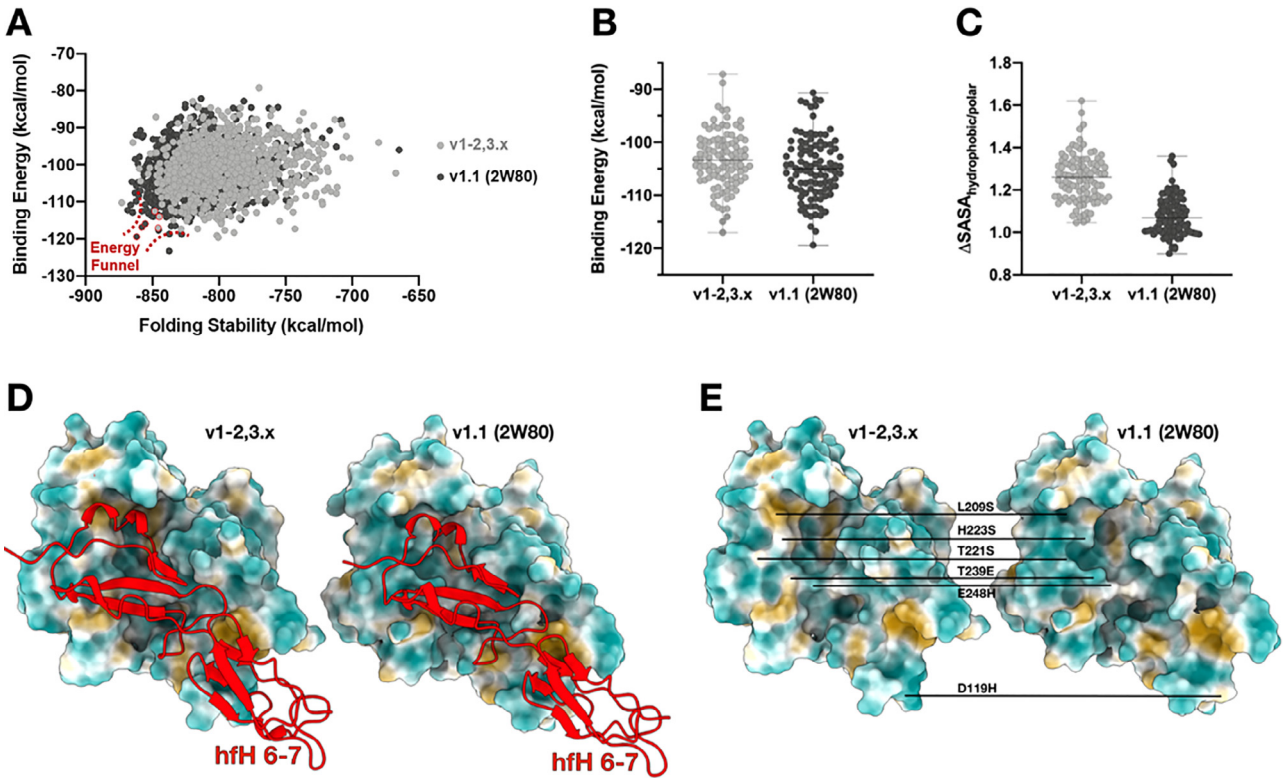

Fig. 7. **A**) Binding energy vs folding stability of 1000 fHbp-hfH complex homology models of variant1 and variant1-2,3.x, calculated using RosettaCM. The lower left quadrant contains the selected top 100 molecular poses, with an energy funnel shown to indicate that the top energetic models (i.e. those with lower energies, based on folding stability and binding energy) are provided by variant1 (dark grey) rather than variant1-2,3.x (pale grey). **B**) Interface energy for top 100 RosettaCM models. The median binding energy for variant1 is −105 kcal/mol, and for variant1-2,3.x is −103 kcal/mol. **C**) Ratio of solvent accessible surface area (ΔSASA) of hydrophobic versus polar interface residues for the top 100 RosettaCM models, showing a median of 1.07 for variant1, and of 1.26 for variant 1–2,3.x. **D**) Surface-cartoon plots of fHbp-hfH complex models (variant1-2,3.x on left, and variant1 on right) with surface colored according to hydrophobicity, (dark golden for the most hydrophobic potentials, through white, to dark cyan for the most hydrophilic) and hfH (domains 6 and 7, from PDB 2w80) in red cartoon. **E**) As in D, without hfH to reveal overall properties of the solvent accessible surface of v1-2,3.x and v1.1. Amino-acid changes located in the hfH interface of the two variants are labelled.

these studies provide a deeper understanding of the detailed and holistic structural and functional nature of this chimeric fHbp molecule, guiding the design of potentially optimized forms.

2.5. Rational design of loss-of-function mutations in fHbp variant1-2,3.x

It has been shown in transgenic mouse models expressing hfH that immunization with engineered non-functional stable forms of fHbp (carrying mutations that reduce their binding to hfH) can elicit higher bactericidal antibody titers than immunization with wild-type fHbp [36,44–46]. Consequently, it has been suggested that a non-functional mutant fHbp antigen that does not bind hfH but that retains immunogenicity might be superior in humans when compared to an fHbp vaccine that binds hfH as normal [12,33,44–48]. However, no such supporting clinical data has yet been reported. Here we sought to enable such studies by designing loss-of-function mutations in fHbp variant1-2,3.x. Using the structural and functional insights accumulated herein, we identified a select few residues (Gln38, Arg41 and His223) as likely key influencers of the interaction between variant1-2,3.x and hfH. These structure-based insights were in agreement with previous reports that mutation in variant1 of Arg41 to Ala or Ser reduced binding to hfH [44], as did the double Ala mutation in variant2 of both Thr221 and His223 [49]. We also combined these structure-based insights with knowledge that the gonococcal orthologue (Ghfp) does not bind hfH (consistent with its natural intracellular localization where it would not encounter hfH) [50–51] and therefore designed variant1-2,3.x molecules carrying the single mutations R41S, H223R, or both Q38A and H223R (Fig. 8A). However, because knock-out mutations in one variant do not necessarily have the same effect in the molecular scaffold of a different variant [49], it was necessary to produce and purify these new recombinant fHbp mutants and test their ability to bind hfH, which was assessed by a surface plasmon resonance (SPR) assay. Indeed, under the conditions used in this simple assay (a full kinetic analysis was not performed), the variant1-2,3.x scaffold carrying either the single mutations R41S or H223R, or the double mutations Q38A/H223R, showed almost no binding to hfH, while the control wild-type variant1 and variant1-2,3.x proteins bound to hfH in line with the kinetic analysis presented above (Fig. 8B). Finally, DSC experiments were performed, demonstrating that these three mutations did not impair thermostability (Fig. 8C), suggesting that these mutant forms of variant1-2,3.x designed for reduced binding to hfH nevertheless maintained excellent biophysical stability properties.

3. Discussion

While some recombinant protein vaccines are effective using only one protein antigen, other multivalent vaccines employ the simultaneous inclusion of multiple antigens in order to successfully elicit broad immune protection against a multitude of circulating pathogenic strains, serotypes or serogroups. However, because of antigen variability, monitoring of the epidemiology is crucial to prompt the design and inclusion of new antigens to overcome any potential reduction in cross-protection. High antigenic sequence variability is exemplified by the *N. meningitidis* virulence

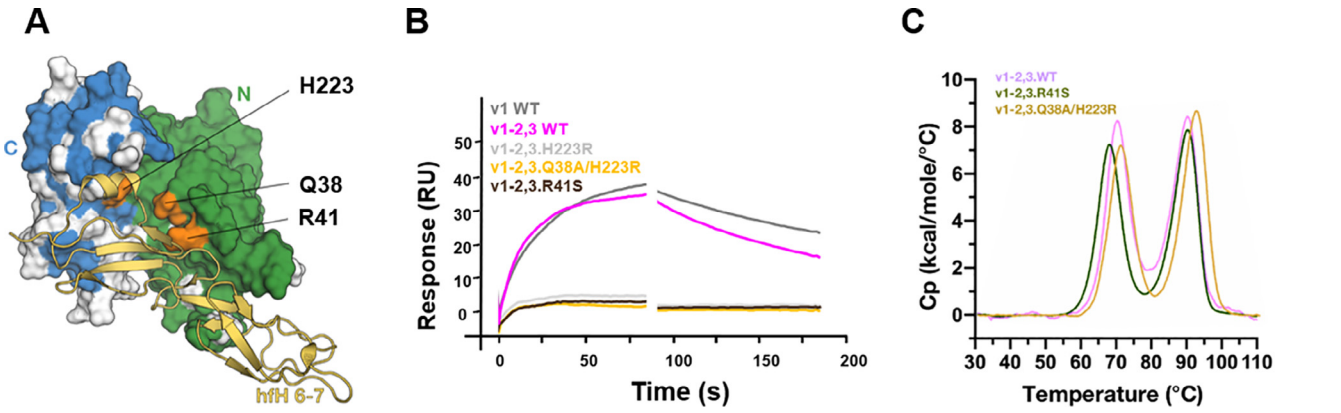

Fig. 8. Rational design of loss-of-function point mutations in fHbp variant1-2,3.x. **A**) A homology model of fHbp v1-2,3.x (surface) bound to hfH domains 6 and 7 (gold cartoon), showing locations of targeted point mutations (orange, labelled). White patches show non-conserved residues between variant1 and variant1-2,3.x. **B**) Experimental SPR sensorgrams showing differential binding to hfH for the wild-type and mutant fHbp variants generated herein. **C**) DSC thermograms of fHbp variant1-2,3.x wild-type (magenta), R41S mutant (brown) and Q38/H223R mutants (orange) show that these three point mutations do not destabilize the scaffold (all T_m values $\geq$ 65 °C (338 K)).

factor known as factor H binding protein (fHbp), of which over 1300 sequence variants are known [13]. The 3D structure of fHbp has been solved and many bactericidal epitopes identified. The availability of so much information has guided the design of more stable and more cross-protective fHbp antigens [22]. Remarkably, the fHbp variant1-2,3.x (from the MenB NL096 strain), is a naturally occurring chimera capable of inducing serum bactericidal activity protective against a wide range of MenB strains [30].

Here, we report the key characteristics of fHbp variant1-2,3.x through an in-depth biochemical and structural analysis relevant for a deeper understanding of fHbp immunological and stability properties. For the vaccinologist, it is worthwhile seeking to understand how evolutionary changes in stability, function and immunogenicity properties driven by "Nature" can influence strain pathogenicity. In the analysis described by Seib *et al.* on 12 different subvariants, the antibodies induced by immunization with the fHbp 1–2,3.x chimera were able to induce complement mediated bactericidal killing for all 11 heterologous strains [30]. Surprisingly, antibodies raised by each of the twelve subvariants were not able to kill the NL096 strain which, notably, was killed only by the homologous sera. These observations suggest that the natural recombination that generated variant1-2,3.x provided the NL096 strain with a unique fHbp chimera retaining all features important for pathogenicity (high stability, efficient factor H binding) and the ability to escape the immune response induced by the most common variants.

While some fHbp variant2 and variant3 antigens are known to have poor thermostability (T_m can be as low as 42 °C (315 K)), here we demonstrated that fHbp variant1-2,3.x has much higher thermostability ($T_m \geq 68 \pm 0.5$ °C (341 K)). This, coupled with growing evidence that thermostability positively correlates with the immunogenicity of protein antigens [31–32,36], suggests that variant1-2,3.x intrinsically has the properties of a potent immunogen.

Herein, we also determined the crystal structure of fHbp variant1-2,3.x at very high resolution (1.2 Å), revealing that it has the canonical overall structure of all fHbp proteins despite fusing together a variant1-like N-terminal domain with a variant2/3-like C-terminal domain. In addition to demonstrating conservation of the two β-barrel folds and their relative orientation, our analysis of the protein surface revealed that this naturally occurring chimeric molecule displays antigenic surfaces that faithfully represent fHbp variant1, variant2 and variant3 proteins, thus encompassing a wide breadth of the highly diverse 'immunogen space' encoded by the many known fHbp sequence variants. The latter may be particularly important for the variant1 moiety, since MenB strains expressing fHbp variant1 have been reported to represent approximately 70% of the circulating strains [38]. These structure-guided observations help to understand, and are in agreement with, the initial demonstration by Seib *et al.* that immunization of mice with variant1-2,3.x can raise a serum antibody response with bactericidal activity against multiple different meningococcal strains, including five strains displaying fHbp variant1 molecules, four strains displaying fHbp variant2, and two strains displaying fHbp variant3 [30]. However, conversely, the NL096 strain is resistant to killing by antibodies raised by variant 1, 2 or 3. These data further suggest that variant1-2,3.x may elicit protection against the vast majority of the circulating meningococcal strains and that the reassortment of fHbp domains is an efficient immune escape mechanism.

Knowledge of sequence and 3D structure can deepen our functional understanding of a protein and can facilitate the tailored design of vaccine antigens with enhanced properties [24–26,52–54]. Upon crystal structure determination and detailed manual and computational analyses of fHbp variant1-2,3.x, we were able to pinpoint a small subset of key residues influencing binding to human factor H (hfH), its natural ligand [55–56]. Such detailed structural information, combined with prior knowledge and novel *in silico* biophysical analyses, allowed a more streamlined approach to the identification of loss-of-function mutations, as compared to a previous study using only homology modelled structures, which implicated over 60 different residues potentially involved in binding hfH [49]. Using site-directed mutagenesis and SPR binding studies, we confirmed two distinct point mutations in fHbp variant1-2,3.x that reduced binding to hfH:R41S and H223R. This structure-based precision design also maintained the high thermostability of these antigens. Immunization experiments in hfH-transgenic mouse models should be performed to further confirm the influence of Factor H binding on the immunogenicity of this antigen.

Collectively, the previous findings of Seib *et al.* [30] together with the data herein demonstrate that the characterization of a rare, naturally occurring antigen can shed more light on its role both as immunogen and virulence factor, revealing the presence of key conserved cross-protective epitopes and mechanisms underlying fHbp-mediated immune escape. Further, sequence- and structure-based analyses of such antigens can enable design of multiple desirable traits, to enable gains in immunogenicity across a range of highly variable pathogenic strains. As we enter an era of ever-expanding genomic and structural information, such

approaches may become more broadly applicable to accelerate a wide range of viral and bacterial vaccine discovery programs.

4. Methods

4.1. Molecular cloning, protein expression and purification

All fHbp proteins (namely, variant1, variant2, variant3, variant1-2,3.x) were cloned into the pET-21b (+) expression vector (Novagen) using NdeI and XhoI or HindIII restriction sites, expressed in *E. coli* BL21 strain DE3 (Invitrogen), and purified via C-terminal hexahistidine tags using metal affinity and ion exchange chromatography steps as described previously [30]. The expression vectors for the following single or double mutant forms of variant1-2,3.x were prepared by the polymerase incomplete primer extension (PIPE) method [57]: Q38A, H223R, Q38A + H223R, R41S, and the mutant proteins were purified as described above. In addition, the variant1-2,3.x sample used for crystallization was further purified by size-exclusion chromatography using a Superdex 75 (16/60) column (GE Healthcare) equilibrated in buffer containing 20 mM Tris-HCl, 150 mM NaCl, pH 8.0, run at a flow rate of 1 ml/min.

4.2. Differential scanning calorimetry (DSC)

The thermal stability of fHbp proteins was assessed by differential scanning calorimetry (DSC) using a MicroCal VP-Capillary DSC instrument (Malvern). The latter instrument operates with high precision as we have demonstrated previously in at least one instance [58], such that an estimated error for each reported T_m value is confidently not more than ± 0.5 °C. fHbp samples were prepared at a protein concentration of 0.5 mg/mL. The DSC temperature scan ranged from 10 °C to 110 °C (283 K-383 K), with a 4 s filter period. Data were analyzed by subtraction of the reference data for a sample containing buffer only, and the curve-fitting procedure was performed using a 2-state model and the Levenberg/Marquardt (LM) non-linear least-square method, as provided within the Origin 7 software.

4.3. Protein crystallization and diffraction data collection and processing

The purified fHbp variant1-2,3.x protein at a concentration of 10 mg/ml was screened with a matrix of 384 crystallization conditions (using JCSG, Morpheus, PEG-Ion and Structure kits) prepared using a Crystal Gryphon robot (Art Robbins Instruments), incubated in a RockImager-182 (Formulatrix) system held at 21 °C. Crystals were obtained after 1 week in crystallization reservoir conditions containing 0.1 M tri-sodium citrate, 3.2 M ammonium sulfate, pH 5.0. Crystals were soaked in the original mother liquor supplemented with 10 % ethylene glycol as cryoprotectant, followed by cryo-cooling in liquid nitrogen. Diffraction of the crystals was tested at the Swiss Light Source (SLS, Villigen, Switzerland) and several full datasets were collected. Diffraction datasets were indexed, integrated and scaled with XDS [59] and Aimless [60], via the CCP4 suite [61]. The structure was solved by molecular replacement with Phaser [62] using as search model template the fHbp variant1 (PDB 3kvd) [63].

4.4. Structure refinement

Initial molecular replacement solutions were subjected to cycles of manual building in Coot [64] and refinement with Phenix.refine [65]. Structure figures were created with Pymol (https://www.pymol.org) and UCSF ChimeraX (Resource for Biocomputing, Visualization and Informatics, University of California, San Francisco) [66]. Surface plots coloured by electrostatic potential were prepared following electrostatic calculations using the APBS method [67]. Structure factors and atomic coordinates have been deposited in the Protein Data Bank (https://www.wwpdb.org) [37] with accession code PDB 7nru.

4.5. Structure modeling and computational analyses

Starting from the previously reported crystal structure of the fHbp variant1-hfH complex (PDB 2w80) [11], a new homology model of the v1-2,3.x-fH complex was prepared using the atomic resolution coordinates of v1-2,3.x for superposition onto 2w80, followed by energy minimization using the Molecular Operating Environment software (MOE, Chemical Computing Group) [68] and Rosetta [43]. The binding interface of the minimized homology model was then inspected both manually and using PISA interface analysis software [39], especially in the regions of non-conserved residues between the two variants, to identify potential factors contributing to the binding affinity differences.

Rosetta comparative modeling (RosettaCM) [43] was used to generate molecular poses for interface analysis. Specifically, three rounds of modeling were performed, both for fHbp variant1 and for variant1-2,3.x. Round 1: All four distinct experimental structures from the asymmetric unit of the fHbp variant1-hfH complex (PDB 2w80) [11] were threaded with either the variant1 or the variant1-2,3.x sequence, generating 1000 models. Round 2: The best model (ranked by folding stability and binding affinity) from Round 1 was modeled 1000 times. Round 3: The final round took the best model from the previous two rounds, and RosettaCM was used to generate 1000 models. The top 100 models (ranked by folding stability), representing the top 3% of molecular poses generated overall, were used for the interface analysis.

4.6. Surface plasmon resonance

Binding experiments were performed using a Biacore T200 instrument (GE Healthcare), equilibrated at 25 °C. Purified full-length hfH (Sigma, Cat. C5813) was covalently-immobilized on a CM-5 sensor chip (GE Healthcare) to a density of 2500 RU, using the standard reagents of freshly mixed N-hydroxysuccinimide (NHS) and 1-ethyl-3-(3-dimethylaminopropyl) carbo-diimide hydrochloride (EDC), with subsequent blocking of any remaining active coupling sites using ethanolamine hydrochloride, according to the manufacturer's instructions. For the titration experiments, fHbp samples were exchanged into the SPR running buffer: HBS-EP+ (10 mM HEPES, 150 mM NaCl, 3 mM EDTA, 0.05 % Surfactant P20 (GE Healthcare)) and five injections were performed with fHbp concentrations in the range of 1 nM to 100 nM, at a flow rate of 40 μL/min. SPR titrations were performed in triplicate. Data were analyzed by subtraction of the reference data for a buffer-only injection, and with curve fitting performed using the Langmuir equation for a 1:1 binding model, as provided in the BIAcore T200 evaluation software. Mean values and standard deviations of the equilibrium dissociation constant (K_D) were determined. For single-injection mode experiments (Fig. 8), the fHbp proteins (wild-types or mutants) were injected at 200 nM protein concentration in phosphate buffered saline (PBS) running buffer at a flow rate of 30 μL/min.

5. Authorship contributions

DV, EM, PLS, WP, VR, NW, SS, MJB designed and/or conducted the studies, including data collection and data analysis. DV, EM and MJB prepared the manuscript draft with important intellectual

input from VM and MP. All authors approved the final manuscript. All authors had full access to the study data.

Funding sources

This study was initiated at Novartis Vaccines & Diagnostics (NVD) Srl which in 2015 became GSK Vaccines Srl (Siena, Italy), part of the GSK group of companies.

Conflicts of interest

All authors were employees of Novartis Vaccines & Diagnostics (NVD) Srl or, later, the GSK group of companies, at the time of the study. The authors DV, EM, VM, MP and MJB are named inventors on patent applications related to fHbp polypeptides. EM, PLS, VM, MP and MJB report ownership of GSK shares.

Acknowledgements

We are grateful to Elena Cartocci, Eva Grassi, Sara Marchi and Maria Scarselli (all employees of GSK) for technical assistance and useful discussions. We thank Joachim Diez and staff of Expose GmbH (Villigen) at the Swiss Light Source (SLS) for their assistance in collecting diffraction data.

References

[1] Pace D, Pollard AJ. Meningococcal disease: clinical presentation and sequelae. Vaccine 2012;30(Suppl 2):B3–9. https://doi.org/10.1016/j.vaccine.2011.12.062.
[2] Rosenstein NE, Perkins BA, Stephens DS, Popovic T, Hughes JM. Meningococcal disease. N Engl J Med 2001;344(18):1378–88. https://doi.org/10.1056/NEJM200105033441807.
[3] ECDC. European Centre for Disease Prevention and Control. Invasive meningococcal disease. ECDC Annual Epidemiological Report, 2017.
[4] Pace D. Quadrivalent meningococcal ACYW-135 glycoconjugate vaccine for broader protection from infancy. Expert Rev Vaccines 2009;8(5):529–42. https://doi.org/10.1586/erv.09.18.
[5] Rappuoli R. Reverse vaccinology, a genome-based approach to vaccine development. Vaccine 2001;19(17–19):2688–91. https://doi.org/10.1016/s0264-410x(00)00554-5.
[6] Seib KL, Scarselli M, Comanducci M, Toneatto D, Masignani V. Neisseria meningitidis factor H-binding protein fHbp: a key virulence factor and vaccine antigen. Expert Rev Vaccines 2015;14(6):841–59. https://doi.org/10.1586/14760584.2015.1016915.
[7] Serruto D, Bottomley MJ, Ram S, Giuliani MM, Rappuoli R. The new multicomponent vaccine against meningococcal serogroup B, 4CMenB: immunological, functional and structural characterization of the antigens. *Vaccine* May 30 2012;30(Suppl 2):B87–97. https://doi.org/10.1016/j.vaccine.2012.01.033.
[8] Zlotnick GW, Jones TR, Liberator P, et al. The discovery and development of a novel vaccine to protect against *Neisseria meningitidis* Serogroup B Disease. Hum Vaccin Immunother 2015;11(1):5–13. https://doi.org/10.4161/hv.34293.
[9] Cantini F, Veggi D, Dragonetti S, et al. Solution structure of the factor H-binding protein, a survival factor and protective antigen of *Neisseria meningitidis*. J Biol Chem 2009;284(14):9022–6. https://doi.org/10.1074/jbc.C800214200.
[10] Mascioni A, Bentley BE, Camarda R, et al. Structural Basis for the Immunogenic Properties of the Meningococcal Vaccine Candidate LP2086. J Biol Chem 2009;284(13):8738–46. https://doi.org/10.1074/jbc.M808831200.
[11] Schneider MC, Prosser BE, Caesar JJ, et al. *Neisseria meningitidis* recruits factor H using protein mimicry of host carbohydrates. Nature 2009;458(7240):890–3. https://doi.org/10.1038/nature07769.
[12] Principato S, Pizza M, Rappuoli R. Meningococcal factor H-binding protein as immune evasion factor and vaccine antigen. FEBS Lett. 2020. https://doi.org/10.1002/1873-3468.13793.
[13] Jolley KA, Maiden MC. BIGSdb: Scalable analysis of bacterial genome variation at the population level. BMC Bioinform. 2010;11:595. https://doi.org/10.1186/1471-2105-11-595.
[14] Masignani V, Comanducci M, Giuliani MM, et al. Vaccination against *Neisseria meningitidis* using three variants of the lipoprotein GNA1870. J Exp Med 2003;197(6):789–99. https://doi.org/10.1084/jem.20021911.
[15] Fletcher LD, Bernfield L, Barniak V, et al. Vaccine potential of the *Neisseria meningitidis* 2086 lipoprotein. Infect Immun 2004;72(4):2088–100. https://doi.org/10.1128/iai.72.4.2088-2100.2004.
[16] Beernink PT, Granoff DM. The modular architecture of meningococcal factor H-binding protein. Microbiology 2009;155(Pt 9):2873–83. https://doi.org/10.1099/mic.0.029876-0.
[17] Pajon R, Beernink PT, Harrison LH, Granoff DM. Frequency of factor H-binding protein modular groups and susceptibility to cross-reactive bactericidal activity in invasive meningococcal isolates. Vaccine 2010;28(9):2122–9. https://doi.org/10.1016/j.vaccine.2009.12.027.
[18] Donald RG, Hawkins JC, Hao L, et al. Meningococcal serogroup B vaccines: Estimating breadth of coverage. Hum Vaccin Immunother 2017;13(2):255–65. https://doi.org/10.1080/21645515.2017.1264750.
[19] Frasch CE, Borrow R, Donnelly J. Bactericidal antibody is the immunologic surrogate of protection against meningococcal disease. Vaccine 2009;27(Suppl 2):B112–6. https://doi.org/10.1016/j.vaccine.2009.04.065.
[20] Beernink PT, Granoff DM. Bactericidal antibody responses induced by meningococcal recombinant chimeric factor H-binding protein vaccines. Infect Immun 2008;76(6):2568–75. https://doi.org/10.1128/IAI.00033-08.
[21] Rippa V, Santini L, Lo Surdo P, et al. Molecular Engineering of Ghfp, the Gonococcal Orthologue of *Neisseria meningitidis* Factor H Binding Protein. Clin Vaccine Immunol 2015;22(7):769–77. https://doi.org/10.1128/CVI.00794-14.
[22] Scarselli M, Arico B, Brunelli B, et al. Rational design of a meningococcal antigen inducing broad protective immunity. Sci Transl Med 2011;3(91). https://doi.org/10.1126/scitranslmed.3002234. 91ra62-91ra62.
[23] Burton DR, Walker LM. Rational vaccine design in the time of COVID-19. Cell Host Microbe 2020;27(5):695–8. https://doi.org/10.1016/j.chom.2020.04.022.
[24] Dormitzer PR, Grandi G, Rappuoli R. Structural vaccinology starts to deliver. Nat Rev Microbiol 2012;10(12):807–13. https://doi.org/10.1038/nrmicro2893.
[25] Graham BS, Gilman MSA, McLellan JS. Structure-based vaccine antigen design. Annu Rev Med 2019;70:91–104. https://doi.org/10.1146/annurev-med-121217-094234.
[26] Kwong PD, DeKosky BJ, Ulmer JB. Antibody-guided structure-based vaccines. Semin. Immunol. 2020;50. https://doi.org/10.1016/j.smim.2020.101428.
[27] Rappuoli R, Bottomley MJ, D'Oro U, Finco O, De Gregorio E. Reverse vaccinology 2.0: Human immunology instructs vaccine antigen design. J Exp Med 2016;213(4):469–81. https://doi.org/10.1084/jem.20151960.
[28] Beernink PT, LoPasso C, Angiolillo A, Felici F, Granoff D. A region of the N-terminal domain of meningococcal factor H-binding protein that elicits bactericidal antibody across antigenic variant groups. Mol Immunol 2009;46(8–9):1647–53. https://doi.org/10.1016/j.molimm.2009.02.021.
[29] Piet JR, Brouwer MC, Exley R, van der Veen S, van de Beek D, van der Ende A. Meningococcal factor H binding protein fHbpd184 polymorphism influences clinical course of meningococcal meningitis. PLoS ONE 2012;7(10):. https://doi.org/10.1371/journal.pone.0047973e47973.
[30] Seib KL, Brunelli B, Brogioni B, et al. Characterization of diverse subvariants of the meningococcal factor H (fH) binding protein for their ability to bind fH, to mediate serum resistance, and to induce bactericidal antibodies. Infect Immun 2011;79(2):970–81. https://doi.org/10.1128/IAI.00891-10.
[31] McLellan JS, Chen M, Joyce MG, et al. Structure-based design of a fusion glycoprotein vaccine for respiratory syncytial virus. Science 2013;342(6158):592–8. https://doi.org/10.1126/science.1243283.
[32] Scheiblhofer S, Laimer J, Machado Y, Weiss R, Thalhamer J. Influence of protein fold stability on immunogenicity and its implications for vaccine design. Expert Rev Vaccines 2017;16(5):479–89. https://doi.org/10.1080/14760584.2017.1306441.
[33] Johnson S, Tan L, van der Veen S, et al. Design and evaluation of meningococcal vaccines through structure-based modification of host and pathogen molecules. PLoS Pathog 2012;8(10):. https://doi.org/10.1371/journal.ppat.1002981e1002981.
[34] Malito E, Faleri A, Lo Surdo P, et al. Defining a protective epitope on factor H binding protein, a key meningococcal virulence factor and vaccine antigen. Proc. Natl. Acad. Sci. USA 2013;110(9):3304–9. https://doi.org/10.1073/pnas.1222845110.
[35] Konar M, Pajon R, Beernink PT. A meningococcal vaccine antigen engineered to increase thermal stability and stabilize protective epitopes. Proc. Natl. Acad. Sci. USA 2015;112(48):14823–8. https://doi.org/10.1073/pnas.1507829112.
[36] Rossi R, Konar M, Beernink PT. Meningococcal factor H binding protein vaccine antigens with increased thermal stability and decreased binding of human factor H. Infect Immun 2016;84(6):1735–42. https://doi.org/10.1128/IAI.01491-15.
[37] Berman H, Henrick K, Nakamura H. Announcing the worldwide Protein Data Bank. Nat Struct Biol 2003;10(12):980. https://doi.org/10.1038/nsb1203-980.
[38] Murphy E, Andrew L, Lee KL, et al. Sequence diversity of the factor H binding protein vaccine candidate in epidemiologically relevant strains of serogroup B *Neisseria meningitidis*. J Infect Dis 2009;200(3):379–89. https://doi.org/10.1086/600141.
[39] Krissinel E, Henrick K. Inference of macromolecular assemblies from crystalline state. J. Mol. Biol. 2007;372(3):774–97. https://doi.org/10.1016/j.jmb.2007.05.022.
[40] Lopez-Sagaseta J, Beernink PT, Bianchi F, et al. Crystal structure reveals vaccine elicited bactericidal human antibody targeting a conserved epitope on meningococcal fHbp. Nat Commun. 2018;9(1):528. https://doi.org/10.1038/s41467-018-02827-7.
[41] Bianchi F, Veggi D, Santini L, et al. Cocrystal structure of meningococcal factor H binding protein variant 3 reveals a new crossprotective epitope recognized by human mAb 1E6. FASEB J. 2019. https://doi.org/10.1096/fj.201900374R. fj201900374R.
[42] Veggi D, Bianchi F, Santini L, et al. 4CMenB vaccine induces elite cross-protective human antibodies that compete with human factor H for binding to meningococcal fHbp. PLoS Pathog 2020;16(10):. https://doi.org/10.1371/journal.ppat.1008882e1008882.

[43] Song Y, DiMaio F, Wang RY, et al. High-resolution comparative modeling with RosettaCM. Structure 2013;21(10):1735–42. https://doi.org/10.1016/j.str.2013.08.005.
[44] Beernink PT, Shaughnessy J, Braga EM, et al. A meningococcal factor H binding protein mutant that eliminates factor H binding enhances protective antibody responses to vaccination. J Immunol 2011;186(6):3606–14. https://doi.org/10.4049/jimmunol.1003470.
[45] Rossi R, Granoff DM, Beernink PT. Meningococcal factor H-binding protein vaccines with decreased binding to human complement factor H have enhanced immunogenicity in human factor H transgenic mice. Vaccine 2013;31(46):5451–7. https://doi.org/10.1016/j.vaccine.2013.08.099.
[46] van der Veen S, Johnson S, Jongerius I, et al. Nonfunctional variant 3 factor H binding proteins as meningococcal vaccine candidates. Infect Immun 2014;82(3):1157–63. https://doi.org/10.1128/IAI.01183-13.
[47] Costa I, Pajon R, Granoff DM. Human factor H (FH) impairs protective meningococcal anti-FHbp antibody responses and the antibodies enhance FH binding. MBio 2014;5(5):e01625–e1714. https://doi.org/10.1128/mBio.01625-14.
[48] Granoff DM, Ram S, Beernink PT. Does binding of complement factor H to the meningococcal vaccine antigen, factor H binding protein, decrease protective serum antibody responses? Clin Vaccine Immunol 2013;20(8):1099–107. https://doi.org/10.1128/CVI.00260-13.
[49] Pajon R, Beernink PT, Granoff DM. Design of meningococcal factor H binding protein mutant vaccines that do not bind human complement factor H. Infect Immun 2012;80(8):2667–77. https://doi.org/10.1128/IAI.00103-12.
[50] Jongerius I, Lavender H, Tan L, et al. Distinct binding and immunogenic properties of the gonococcal homologue of meningococcal factor h binding protein. PLoS Pathog 2013;9(8):. https://doi.org/10.1371/journal.ppat.1003528e1003528.
[51] Veggi D, Gentile MA, Cantini F, et al. The factor H binding protein of *Neisseria meningitidis* interacts with xenosiderophores *in vitro*. Biochemistry 2012;51(46):9384–93. https://doi.org/10.1021/bi301161w.
[52] Crank MC, Ruckwardt TJ, Chen M, et al. A proof of concept for structure-based vaccine design targeting RSV in humans. Science 2019;365(6452):505–9. https://doi.org/10.1126/science.aav9033.
[53] Malito E, Carfi A, Bottomley MJ. Protein Crystallography in Vaccine Research and Development. Int J Mol Sci 2015;16(6):13106–40. https://doi.org/10.3390/ijms160613106.
[54] Saylor K, Gillam F, Lohneis T, Zhang C. Designs of antigen structure and composition for improved protein-based vaccine efficacy. Front Immunol 2020;11:283. https://doi.org/10.3389/fimmu.2020.00283.
[55] Ingram G, Hakobyan S, Hirst CL, et al. Complement regulator factor H as a serum biomarker of multiple sclerosis disease state. Brain 2010;133(Pt 6):1602–11. https://doi.org/10.1093/brain/awq085.
[56] Perkins SJ, Nan R, Li K, Khan S, Miller A. Complement factor H-ligand interactions: self-association, multivalency and dissociation constants. Immunobiology 2012;217(2):281–97. https://doi.org/10.1016/j.imbio.2011.10.003.
[57] Klock HE, Lesley SA. The Polymerase Incomplete Primer Extension (PIPE) method applied to high-throughput cloning and site-directed mutagenesis. Methods Mol. Biol. 2009;498:91–103. https://doi.org/10.1007/978-1-59745-196-3_6.
[58] Liguori A, Malito E, Lo Surdo P, et al. Molecular basis of ligand-dependent regulation of NadR, the transcriptional repressor of meningococcal virulence factor NadA. PLoS Pathog 2016;12(4):. https://doi.org/10.1371/journal.ppat.1005557e1005557.
[59] Xds KW. Acta Crystallogr D Biol Crystallogr 2010;66(Pt 2):125–32. https://doi.org/10.1107/S0907444909047337.
[60] Evans PR, Murshudov GN. How good are my data and what is the resolution? Acta Crystallogr D Biol Crystallogr 2013;69(Pt 7):1204–14. https://doi.org/10.1107/S0907444913000061.
[61] Winn MD, Ballard CC, Cowtan KD, et al. Overview of the CCP4 suite and current developments. Acta Crystallogr D Biol Crystallogr 2011;67(Pt 4):235–42. https://doi.org/10.1107/S0907444910045749.
[62] McCoy AJ, Grosse-Kunstleve RW, Adams PD, Winn MD, Storoni LC, Read RJ. Phaser crystallographic software. J Appl Crystallogr 2007;40(Pt 4):658–74. https://doi.org/10.1107/S0021889807021206.
[63] Cendron L, Veggi D, Girardi E, Zanotti G. Structure of the uncomplexed *Neisseria meningitidis* factor H-binding protein fHbp (rLP2086). Acta Crystallogr Sect F Struct Biol Cryst Commun 2011;67(Pt 5):531–5. https://doi.org/10.1107/S1744309111006154.
[64] Emsley P, Lohkamp B, Scott WG, Cowtan K. Features and development of Coot. Acta Crystallogr D Biol Crystallogr 2010;66(Pt 4):486–501. https://doi.org/10.1107/S0907444910007493.
[65] Afonine PV, Grosse-Kunstleve RW, Echols N, et al. Towards automated crystallographic structure refinement with phenix.refine. *Acta Crystallogr D Biol Crystallogr*. Apr 2012;68(Pt 4):352-67. doi:10.1107/S0907444912001308.
[66] Goddard TD, Huang CC, Meng EC, et al. UCSF ChimeraX: Meeting modern challenges in visualization and analysis. Protein Sci 2018;27(1):14–25. https://doi.org/10.1002/pro.3235.
[67] Baker NA, Sept D, Joseph S, Holst MJ, McCammon JA. Electrostatics of nanosystems: application to microtubules and the ribosome. Proc. Natl. Acad. Sci. USA 2001;98(18):10037–41. https://doi.org/10.1073/pnas.181342398.
[68] *Molecular Operating Environment (MOE)*. 2019.